Role of pressure-induced stacking faults on the magnetic properties of gadolinium

Rafael Martinho Vieira,[1,2] Olle Eriksson,[1] Alena Vishina,[1] Torbjörn Björkman,[2] Ondřej Šipr,[3,4,*] Patrik Thunström,[1] and Heike C. Herper[1]

[1]*Department of Physics and Astronomy, Uppsala University, Box 516, SE-751 20 Uppsala, Sweden*
[2]*Physics, Faculty of Science and Engineering, Åbo Akademi University, FI-20500 Turku, Finland*
[3]*FZU-Institute of Physics of the Czech Academy of Sciences, Cukrovarnická 10, CZ-160 00 Prague, Czech Republic*
[4]*New Technologies Research Centre, University of West Bohemia, CZ-301 00 Pilsen, Czech Republic*

(Received 6 September 2023; revised 13 September 2024; accepted 7 October 2024; published 4 November 2024)

Experimental data show that under pressure, Gd goes through a series of structural transitions hcp → Sm-type (close-packed rhombohedral) → dhcp that is accompanied by a gradual decrease of the Curie temperature and magnetization till the collapse of a finite magnetization close to the dhcp structure. We explore theoretically the pressure-induced changes of the magnetic properties, by describing these structural transitions as the formation of fcc stacking faults. Using this approach, we are able to describe correctly the variation of the Curie temperature with pressure, in contrast to a static structural model using the hcp structure.

DOI: 10.1103/PhysRevB.110.174404

I. INTRODUCTION

Being the elemental metal with the highest known atomic spin moment at low temperature, Gd seized early the attention of the magnetism community, and its properties are very well documented [1,2]. Several studies of its magnetic, structural, and spectroscopic properties have been reported, from experiments and theory. Within the existing literature on first-principles calculations for Gd, it is possible to find different treatments of the f states and their respective impact on the electronic band structure [3,4]. In conjunction with other studies on magnetic properties such as magnetic moment [5,6], the exchange parameters [3,4], magnetic anisotropy [7], and magnetic entropy [8], they have proven to be critical for the description of the fundamental magnetic phenomena and establish a solid background on the capabilities and limitations of *ab initio* methods in studying Gd.

Recently, there has been a discussion of the magnetic properties of Gd under pressure [9–12]. Experiments report a gradual decrease in the magnetization and the Curie temperature till around 6 GPa, where the magnetization collapses [10,11,13–17], attributing generally such collapse to a shift in the magnetic ordering from ferromagnetic (FM) to antiferromagnetic (AFM).

Accompanying the changes in the magnetic properties in Gd under pressure, there are also changes in the crystal structure. At around 2 GPa the structure is reported to go from hexagonal close packed (hcp) to a Sm-type structure (9R) and then at 6.5 GPa, close to where the magnetization collapses, there is a structural transformation to a double-hexagonal-close-packed structure (dhcp). The coupling between the magnetic and structural properties has not been investigated in detail, which is the motivation behind the present investigation.

In this work, we show that pure volumetric effects alone do not explain the pressure-induced variations of the magnetic properties. This is in agreement with a previous theoretical study [9], which found a strong coupling between the stability of the high-pressure structures and the magnetic properties. This work implied that structural changes along the transformation path hcp → Sm-type (9R) → dhcp strongly impact the magnetic properties. In this work, we elucidate this finding by means of *ab initio* electronic structure theory, coupled with atomistic spin simulations.

The dhcp, hcp, and 9R structures are hexagonal stacked structures that result from a repeating pattern of A, B, and C stacked hexagonal layers with slightly different arrangements of atoms. Depending on the arrangement of these layers, either fcc or hcp environments are formed. For example, the hcp structure (ABAB stacking) contains only sites with hcp environments, while the 9R structure (ABABCBCAC stacking) comprises six sites with a hcp environment and three sites with a fcc environment [see Fig. 1(a)]. In the dhcp structure (ABAC stacking), there exist two sites with a hcp environment and two others with a fcc environment.

Since these structures differ primarily in the ratio of hcp-fcc environments, one can describe the observed, pressure-induced transformation from hcp to Sm-type to the dhcp structure as the formation/accumulation of fcc stacking fault structures [18]. This picture is compatible with experiment [19]; e.g., the equation of state does not exhibit any drastic variation of the volume or elastic properties at the transition pressures, indicating their second-order nature. Moreover, this perspective can be considered a valuable

*Deceased.

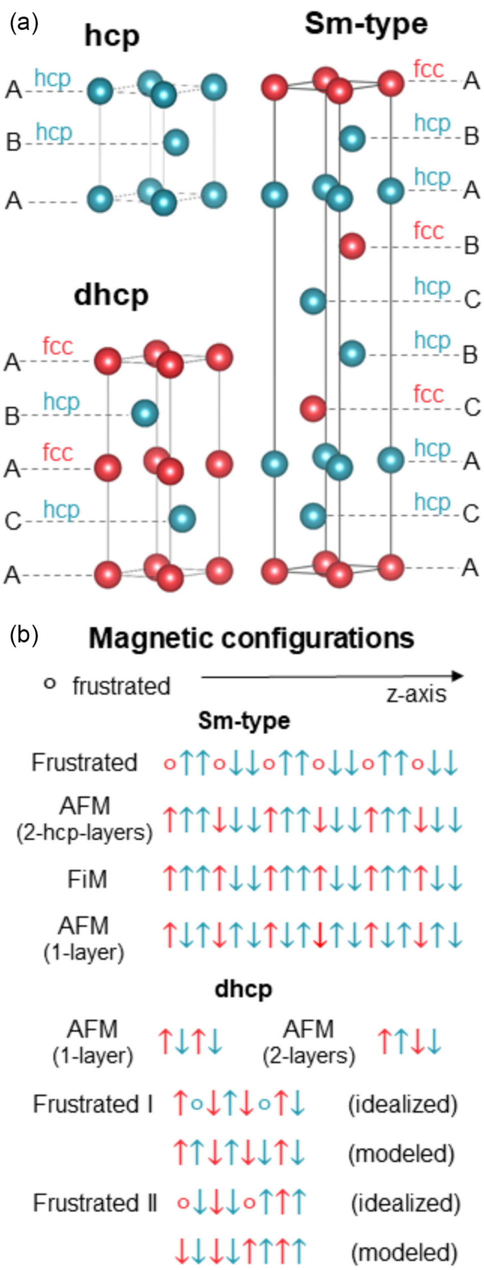

FIG. 1. (a) Schematic picture of hcp (blue) and fcc (red) environments in the Gd structures considered. Structures generated with VESTA [36]. (b) Diagram of different magnetic configurations considered in the Sm-type (top) and dhcp structures. In the Sm-type, the frustrated configuration refers to the experimental magnetic order [10], which we analyze using the CPA-DLM method.

addition to the existing explanation of coexisting phases expanding or contracting under pressure, as it offers insight into the interface between these phases. The formation and accumulation of periodic stacking fault structures with an fcc arrangement possess a subtle signature structure, making it challenging to differentiate them from systems exhibiting coexisting phases, as detailed in Appendix A.

The appeal of this description of formation/accumulation of stacking faults lies in its ability to allow for a simplified model of the structural changes and reformulates the problem in terms of a relationship between the magnetic properties of Gd and the presence of fcc stacking faults. In the following, we explore this possibility to explain the observed pressure dependence of the magnetization and Curie temperature.

II. MATERIALS AND METHODS

A. Computational details

Density functional theory (DFT) calculations of the magnetic and electronic structure were made using the RSPt code [20], a full-potential linear muffin-tin orbital (FP-LMTO) method. Calculations are performed within the local spin density approximation (LSDA) [21] and the f electrons are treated as spin-polarized core states (open-core approximation). This setup has been shown to avoid artificial hybridization of f states with d electrons seen in simple DFT calculations of hcp Gd [3]. Moreover, in Ref. [9], it was observed that the treatment of f electrons does not play a role in structural stability, so we found it reasonable to use the same setup for the Sm-type and the dhcp structures. In Appendix B we briefly discuss results from DFT combined with dynamical mean field theory (DMFT) calculations within the Hubbard-I approximation, which support this choice. The package CIF2Cell was used in the preparation of the DFT input files [22].

To compare the energies of various magnetic configurations, including those with magnetic disorder in fcc sites, additional calculations were performed using the KKR method [23,24] as implemented in the SPR-KKR method [25]. The magnetic disorder was modeled using the disordered local moment (DLM) approach and treated using the coherent potential approximation (CPA) [26,27]. For this set of calculations, f states were treated within the LSDA+U correction in the rotationally invariant formulation [28] with $U = 6.7$ eV and $J = 0.7$ eV [4].

Using the RSPt software we calculated the Heisenberg exchange couplings, J_{ij}, within the LKAG formalism [29,30] including *spd* orbitals, which we used as input for Monte Carlo (MC) simulations performed within the UppASD code [31,32] in order to capture the temperature effects of the magnetic properties. In the MC simulations, we made use of the conventional atomistic Heisenberg Hamiltonian:

$$\mathcal{H} = -\frac{1}{2}\sum_{i\neq j} J_{ij}\mathbf{e_i}\cdot\mathbf{e_j} - \sum_i \mathbf{H}\cdot\mathbf{m_i}, \tag{1}$$

which describes the pair exchange interactions between magnetic moments ($\mathbf{m}$) pointing along unit vectors ($\mathbf{e}$), and the interaction of the magnetic moments with an external magnetic field ($\mathbf{H}$). We considered the total site magnetic moment, including *spdf* orbitals. The MC simulations were performed for the hcp as described in Ref. [8], while for the dhcp and Sm-type phases, we considered a simulation box with a minimum of approximately $\approx 83\,000$ sites and 75 000 MC steps with the Metropolis algorithm.

B. Model structures

Whereas the hcp phase of Gd is known to have a ferromagnetic (FM) ordering, the Sm-type and dhcp phases have been suggested to be antiferromagnetically (AFM) ordered

TABLE I. Summary of the structural and magnetic properties from the DFT (FP-LMTO) calculations at ambient conditions. In hcp two different AFM patterns were considered: the 1-layer ↑↓↑↓ and the 2-layer ↑↑↓↓ patterns. A similar pattern was considered for the Sm-type and dhcp structures, as shown in Fig. 1.

Phase	a (Å)	c/a	$\langle m_{site} \rangle$ (μ_B)	ΔE_0 (mRy/atom)
		hcp		
FM	3.642 [8]	1.60	7.59	0
AFM (1-layer)			7.44	3.57
AFM (2-layer)			7.53	2.31
		Sm-type		
AFM (1-layer)	3.618 [34]	14.43	7.41	1.38
AFM (2-layer)			7.49	0
FiM			7.49	0.01
FM			7.53	0.31
		dhcp		
FM	3.402 [35]	3.25	7.41	0.25
AFM (1-layer)			7.37	0.65
AFM (2-layer)			7.41	0
AFM (frustrated I)			7.37	0.65
AFM (frustrated II)			7.41	0.11

between pairs of the hexagonal planes (A-type AFM) [9,10]. Hence, we compared the ground-state energies and magnetic properties of the FM/AFM configurations for the structures under pressure.

The AFM configuration is incommensurate with the Sm-type structure, becoming nontrivial in how the moments in fcc-environment sites are aligned. They either become magnetically frustrated [9,10] or one has to consider a magnetic unit cell that is twice the structural unit cell, to achieve a lattice that has a proper periodicity of the structure and magnetic properties.

Neutron diffraction data suggest that in the Sm-type structure, the hcp layers form an AFM pattern with two parallel aligned layers (AFM 2-layer), ↑↑ o ↓↓, intercalated by the fcc layers (o) with frustrated magnetism [10]. With this configuration in mind, we explored the stability of possible AFM arrangements [see Fig. 1(b)] in the DFT calculations. Additionally, we included a ferrimagnetic-like (FiM) configuration, where magnetic moments at the fcc sites have all the same orientation and can be seen as an AFM state with a magnetic defect (caused by the magnetic frustration). While not entirely conclusive, the neutron diffraction data in Ref. [10] hint at a peak of magnetic origin that can be associated with the (0, 0, 15/2) plane. Within the dhcp structure, the magnetic propagation vector associated with this peak fits the patterns [33] presented in Fig. 1(b). In the DFT calculations for the dhcp structure, we modeled these configurations, resolving the magnetic ordering in the frustrated sites antiparallel between them. In this way, we fit the total magnetic moment to zero, in agreement with the experimental observations.

The lattice parameters of the structures considered and magnetic moments resulting from the FP-LMTO calculations at ambient conditions are summarized in Table I. As in other calculations [9], we observe only a tiny variation in the local magnetic moments when different magnetic and structural arrangements are considered. In the case of the Sm-type structure, we observe in Table I that the AFM (2-layer) state with a doubled structural unit cell has the lowest energy of all arrangements considered in FP-LMTO calculations. This AFM pattern on the hcp layers is consistent with previous findings [10]. However, the very similar energy of the FiM state shows that low-lying, possibly noncollective magnetic excitations are possible for this polymorph. In the KKR-CPA calculation, the ground state is found to be FM instead, but we observe similar energies for the AFM 2-layer ($\Delta E_0 = 1.53$ mRy/atom) and FiM states ($\Delta E_0 = 1.59$ mRy/atom). We associate the disagreement in the ground state between codes as a result of different approximations and technicalities involved in both methods and accept the FP-LMTO results as a reference due to the general better description obtained in full-potential methods. More importantly, we observe that magnetic frustration in the fcc sites (with DLM moments) is not energetically favorable for either FM or AFM configurations. We focus on this last result, as the similarity between the configurations allows for a better comparison of the energies calculated in the KKR-CPA method. This result, combined with the exchange parameters presented ahead, suggests that the magnetic frustration predicted experimentally [10] does not manifest with the frustrated layers adopting a paramagnetic configuration. Instead, our results suggest that a frustrated layer retains its magnetic order within the layer, but does not align in a periodic pattern along the stacks.

In the case of the dhcp structure, we observe the double-layer AFM configuration to be the ground state, similar to the Sm-type structure. The small energy differences between various magnetic configurations hint at a complex magnetic arrangement, with local magnetic excitations.

III. RESULTS AND DISCUSSION

A. Exchange parameters

The exchange parameters (J_{ij}) of the three investigated structures (hcp, Sm-type, dhcp) obtained for the respective magnetic DFT ground-state configuration are given in Fig. 2. These values serve as input for the subsequent Monte Carlo simulations. The J_{ij} values show similarities between phases, with the most significant disparity being the presence of strong long-range AFM couplings in the region $1.7 < d/a < 2.0$ for the Sm-type and dhcp phases. Such couplings are likely responsible for de-stabilizing a pure FM order in these structures under pressure. A similar increase in the strength of AFM exchange is observed for elemental Nd when comparing the dhcp phase against the hcp structure [37], which was argued to be responsible for the self-induced spin-glass state of this system. In general, for the dhcp and Sm-type structure, we observe that coupling between first neighbors that appears between an fcc site and an hcp site is weaker than couplings between atoms that both are at hcp sites. Furthermore, we observe in all phases the oscillatory behavior of the J_{ij} that characterizes RKKY interactions. The frequency of these oscillations is smaller in the dhcp phase compared to the Sm-type and hcp phases [see Fig. 2(b)].

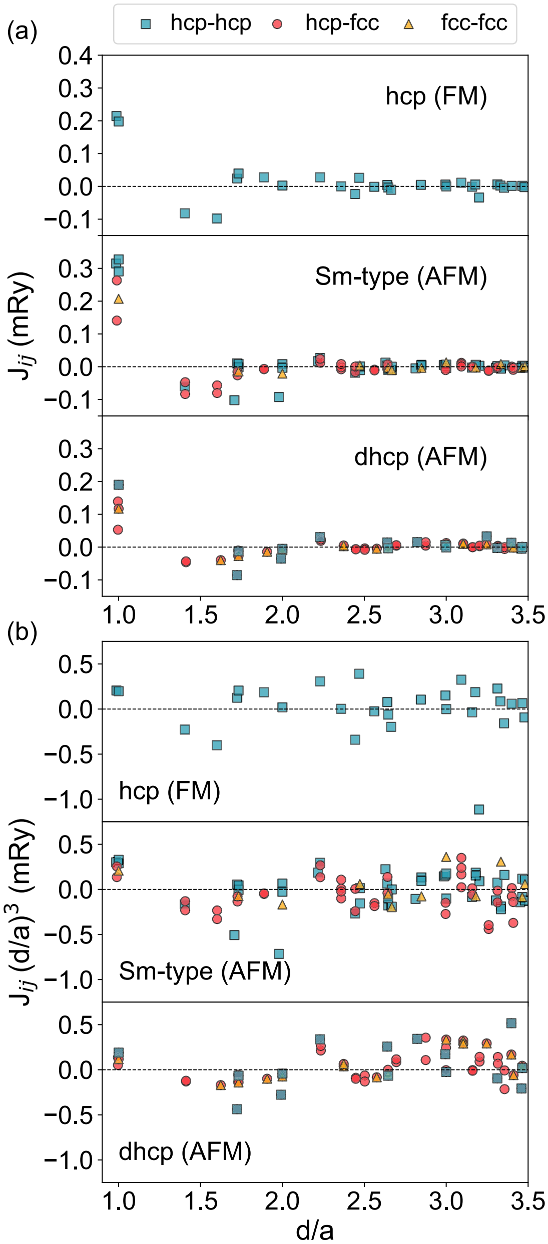

FIG. 2. (a) Exchange parameters for Gd in the hcp (top), Sm-type (middle), and dhcp (bottom) structures obtained from the respective ground states according to DFT calculations (double-layer AFM for both Sm-type and dhcp). (b) Equivalent to (a) with a prefactor $(d/a)^3$ on the exchange parameters, to highlight the RKKY interaction. The interaction between different types of sites in the stacking sequence is given as hcp-hcp, hcp-fcc, and fcc-fcc.

In Ref. [15] it is pointed out that the reduction of the lattice parameter by pressure will lower the bottom of the conduction band leading to a decrease in the density of states at the Fermi level [$D(\epsilon_F)$]. Since the strength of RKKY interactions is proportional to $D(\epsilon_F)$ [15], this would lead to the decrease of exchange interactions and hence to a lower T_C. In our first-principles calculations for compressed volumes of the hcp structure (see Table II), we do indeed observe a reduction of the $D(\epsilon_F)$ that is accompanied by a decrease of the T_C (e.g., as calculated from mean-field theory; see blue circles in Fig. 3). However, as this figure shows, the pressure dependence of the theoretical values is significantly less pronounced than in the experiment. Additionally, for higher pressures, between 4 GPa and 6 GPa, $D(\epsilon_F)$ increases with the volume reductions, due to intricate details of the electronic structure, while the respective calculation for T_C decreases. This implies that the variation of the RKKY interactions solely by volumetric effects, within the hcp phase, does not explain the observed experimental trend for T_C.

TABLE II. Density of states at the Fermi level vs pressure (volumetric variations only) in the hcp structure of Gd. The relation between pressure and lattice parameter was determined using the Murnaghan equation of state in the calculations described in Appendix C.

Pressure (GPa)	$D(\epsilon_F)$ (mRy/state/atom)
0	12.25
2	11.96
4	11.44
6	11.86
8	12.73

An interesting aspect is that we observe a significant increase in the strength of the first and second nearest neighbors' exchange interactions (FM) between atoms in hcp-like environments for the Sm-type structure in comparison to the hcp structure. This result seems counterintuitive since the experimental trend for T_C with pressure ($dT_C/dP < 0$) would suggest that the decrease of T_C is a consequence of the

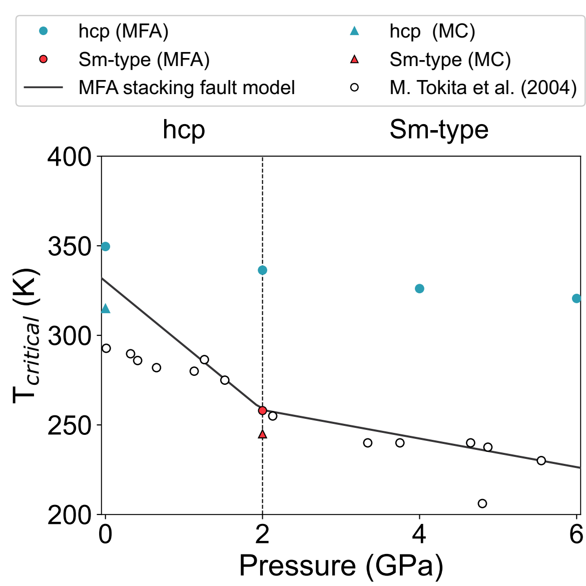

FIG. 3. Critical temperature variation with pressure. Open circles refer to experimental data extracted from Ref. [15], while filled circles are mean-field approximations of T_C from the *ab initio* exchange parameters. The triangles correspond to the critical temperature calculated from the Monte Carlo simulations. A solid line is used for the mixing model for hcp and fcc stacks to estimate T_C (for more details we refer to the text).

weakening of the ferromagnetic couplings. We observe that instead, an increase in AFM couplings is responsible for the decrease in the ordering temperature; see Fig. 2. Nevertheless, this set of exchange parameters allows us to determine an order-disorder transition temperature close to experimental observations.

B. Monte Carlo simulations

Materials with comparable FM and AFM couplings tend to develop more complex magnetic configurations, such as spin spirals or spin glasses, in order to balance these competing alignments [37]. For simplicity, we assume collinear configurations in the DFT calculation. However, the J_{ij} parameters calculated for these configurations should capture this competition between FM-AFM couplings and can therefore be used in MC simulations to get a more realistic picture of the magnetic configuration. This analysis is particularly interesting for the Sm-type and dhcp structures due to the significant AFM couplings which resulted from these calculations; see Fig. 2. To examine the relaxed magnetic configuration in the MC simulations, we also determined the distribution of magnetic moment components across the various sites within the simulation box, as illustrated in the histograms presented in Fig. 4.

Experimentally, a large magnetization is measured for the Sm-type phase, comparable to the hcp phase [10,15,38] ($\approx 7.5\mu_B$), which is not in agreement with the AFM ground state given by the collinear DFT calculations, as reported in Table I. A few scenarios can be proposed to explain these contrasting results. In systems with noncollinear ordering (e.g., magnetic canting), a finite magnetization can arise even in the AFM configuration. However, in such cases, it is unlikely that the magnetization would be as high as the one observed experimentally.

A more likely scenario is that a FM configuration is stabilized by the influence of an external magnetic field or finite-temperature effects. Moreover, if the hcp and Sm-type phases coexist, the hcp phase can stabilize a FM configuration in the composite. In a simplified model, the magnetization of the hcp phase can be seen as acting like an external magnetic field on the Sm-type phase. For this reason, we considered two possible setups in the Monte Carlo simulations. First, we simulated a field-free relaxation, guided only by the exchange parameters corresponding to the pure Sm-type phase. Afterward, we proceeded with a MC relaxation under a magnetic field of 2.75 T, which is the magnitude of the magnetic field generated by the ordered moments in the hcp phase, to describe the case of coexistence of hcp and Sm-type phases, with the latter embedded in the former. Thus the interaction between phases is modeled only by the magnetostatic field induced by the hcp magnetization. Applying an external field is also more realistic for comparison of the calculated magnetization to measurements later.

In the field-free simulation, no finite magnetization is obtained in the Sm-type phase in the temperature range of 1 to 300 K; see Fig. 5. The spin distribution shown in Fig. 4(a) appears to be roughly an AFM configuration with some degree of disorder but with a clear general orientation of spins. In contrast to that, the setup with applied external magnetic field

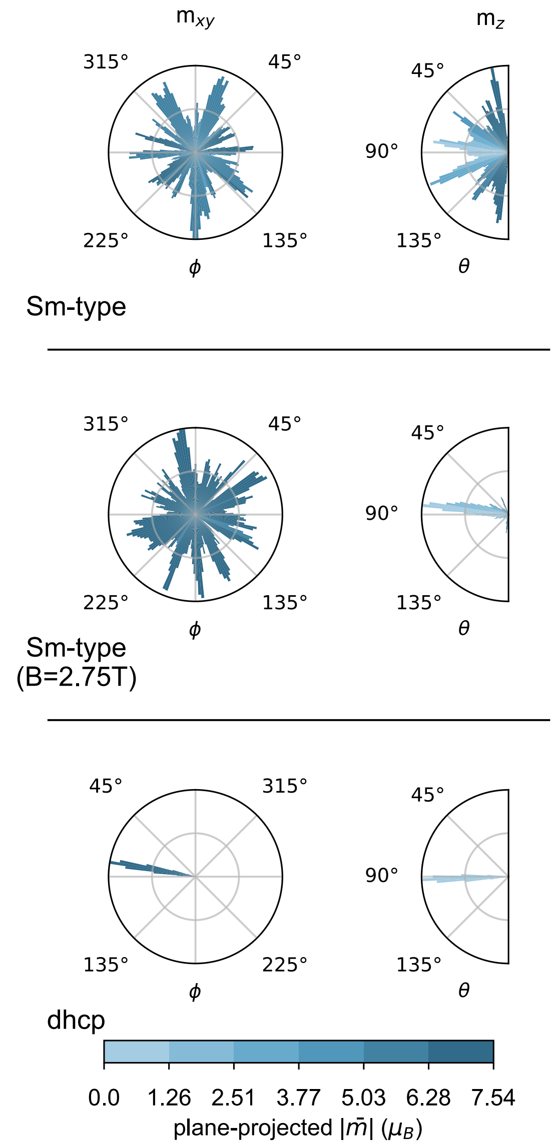

FIG. 4. Statistical distribution of spin directions (spherical coordinates with azimuthal angle ϕ in the x-y plane and polar angle θ) for different Gd systems simulated in classical Monte Carlo simulations at $T = 1$ K with UppASD. The bars are colored according to the average magnetic moment (projected in the respective x-y or z plane) of the spins aligned in the respective direction.

results in a configuration with a magnetization of roughly 1 μ_B per atom [Figs. 4(b) and 5]. The magnetic field breaks the symmetry, giving rise to a finite induced magnetic moment, while simultaneously increasing the spin disorder in the perpendicular plane; see Fig. 4(b). The calculated heat capacity (see Appendix E) in the simulation range of 1 to 300 K reveals that both sets of calculations have critical temperatures of around 245 K. Both setups also share a smaller peak on the heat capacity of around 100 K. This smaller peak suggests that there is a new magnetic regime likely to be caused by temperature fluctuations overcoming one (or a set of) significant exchange couplings.

A further increase of the pressure leads to the collapse of a magnetically ordered state with finite magnetization and then

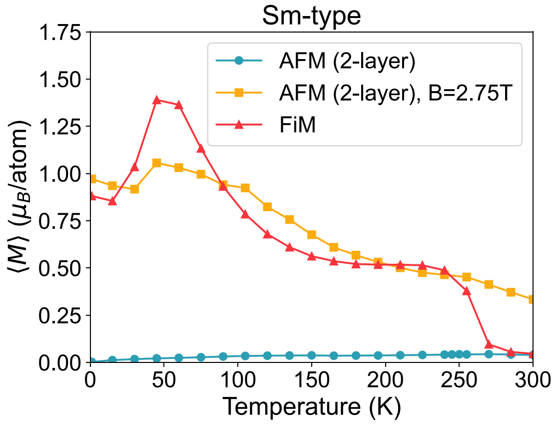

FIG. 5. Temperature-dependent magnetization curves simulated with Monte Carlo in UppASD for different sets of J_{ij} calculated for different magnetic configurations of Gd in the Sm-type structure.

a transition to the dhcp phase. In this phase, we observed that although the DFT energies for the dhcp phase predict an AFM configuration, the MC simulations converge in a FM configuration with the magnetic moment aligned in the *x*-*y* plane, in disagreement with experiments. In some cases, discrepancies between magnetic configurations obtained directly from DFT calculations and configurations obtained from corresponding MC simulations for DFT-derived J_{ij} coupling constants suggest that DFT calculations may not have converged to the ground state. Instead, the magnetic configuration from the MC simulations should be considered for the DFT computations, as it can minimize the energy. However, in this case, we confirm that this is not the case, as the energy of the FM configuration is higher than that of the AFM (2-layer) configuration. Additionally, we observe a similar disagreement using the J_{ij} set calculated for the FM configuration, which relaxes into AFM during MC simulations (more details in Appendix D). Due to the small energy difference between magnetic configurations (see Table I), we infer that the system is magnetically frustrated, potentially due to constraints imposed by the collinear description in DFT or intrinsic properties, similar to what occurs in the case of Nd (dhcp) [37].

C. Stacking fault effects

In the mean-field approximation (MFA), one can estimate the ordering temperature as

$$T_{\text{critical}} = \frac{2J_0}{3k_B}, \tag{2}$$

where $J_0 = \sum_j J_{0j}$ corresponds to the sum of the exchange interaction energies [39]. For structures with stacking faults (such as the Sm-type structure), one may identify at least two sets of J_{ij} associated with either hcp or fcc sites. Thus, we can split J_0 in Eq. (2) into two terms, one containing the sum of all exchange interactions located in fcc sites (including then $J_{fcc-fcc}$ and $J_{fcc-hcp}$ couplings), J_0^{fcc}, and the sum of all exchange interactions located in hcp sites (including then $J_{hcp-hcp}$ and $J_{hcp-fcc}$ couplings), J_0^{hcp}. The two terms are summed, taking into account the fraction of the respective stacking environment; e.g., in the case of the Sm-type structure, which is composed of 2/3 hcp sites and 1/3 fcc sites, we use $J_0 = 0.6\bar{6}J_0^{hcp} + 0.3\bar{3}J_0^{fcc}$, which is then used in Eq. (2) to estimate the ordering temperature. Note that Eq. (2) is suitable for systems with one magnetic sublattice, but since we distinguish the fcc and hcp sites having distinct J_{ij} sets we have in practice two sublattices. In such cases, the correct procedure for estimation of T_C within the mean-field approximation requires the computation of the highest eigenvalue of the Heisenberg Hamiltonian [see Eq. (1)] [40]. Yet, due to their similar properties (magnetic moment and coordination), Eq. (2) yields reasonable results for the Sm-type phase with only minor discrepancies when compared to the exact approach.

Extending this idea to other stacking structures, we propose to evaluate J_0 as an average of both fcc and hcp environments:

$$J_0 = xJ_0^{hcp} + (1-x)J_0^{fcc} \tag{3}$$

with x being the ratio of the number of hcp layers in the structure. This linear interpolation approach aligns with the accumulation model of fcc stacking faults, serving as the transition mechanism between the hcp to Sm-type and dhcp structures. While the exact relationship remains to be determined, we have chosen a linear relationship as the simplest assumption. Moreover, the linear relation is also justified by the physical characteristics of the structures considered. Our J_{ij} calculations show that the interaction between layers weakens rapidly with distance (see Fig. 2). Also, we notice that, in general, interactions involving fcc layers are not as strong as pure hcp-hcp interactions. Given that there are no adjacent fcc layers in hcp, Sm-type, and dhcp structures, it becomes clear that fcc layers interact weakly with each other. Thus, the impact of fcc stacking faults on magnetic properties can be approximated to minor perturbations. By combining Eqs. (3) and (2), we obtain a MFA model for T_{critical} dependence on stacking faults:

$$T_{\text{critical}} = \frac{2}{3k_B}\left[xJ_0^{hcp} + (1-x)J_0^{fcc}\right] = xT_C^{hcp} + (1-x)T_C^{fcc} \tag{4}$$

with the magnetic ordering temperature given by a weighted average of the T_C for hcp and fcc layers. We highlight that our approach is analogous to the application of the virtual crystal approximation (VCA) [41] to describe alloy behavior. However, instead of considering chemical mixing, there is mixing of fcc and hcp layers.

To be able to study the pressure dependence of the transition temperature based on Eq. (4), we need a model that relates the fraction of hcp layers, x, and fcc layers, $(1-x)$, to the applied pressure. As an approximate description, we consider a linear decrease of x with pressure, with a different decrease ratio between the transition ranges (validity shown in Appendix C). Specifically, when transitioning from the hcp phase (where $x = 1$ and is stable at $P = 0$ GPa) to the Sm-type phase (where $x = 2/3$ and is stable at $P = 2$ GPa), the decrease ratio has one value, $0.1\bar{6}$ stacks/GPa. When transitioning from the Sm-type phase to the dhcp phase (where $x = 1/2$ and is stable above $P = 6.5$ GPa), a different decrease ratio is applicable, $0.\overline{037}$ stacks/GPa.

We used this relationship between pressure and the formation of stacking faults, combined with Eq. (4) and the J_0^{hcp} and J_0^{fcc} calculated for the Sm-type structure, to evaluate the variation of T_{critical} with pressure. Employing the J_{ij} obtained for the Sm-type is motivated by the coexistence of both hcp and fcc sets in the phase and for being roughly the expected structure throughout the majority of the pressure range that was explored (0–6 GPa).

The calculated T_{critical} values are in good agreement with experimental findings reported in Ref. [15], as shown in Fig. 3.

Here, the agreement in the pressure range of the Sm-type structure (2–6.5 GPa) supports the hypothesis of the formation of fcc stacking faults under pressure as the primary mechanism for the T_{critical} variation observed experimentally. The pressure change of the ordering temperature from a model that only considers a volume variation of a stacking-fault-free hcp phase is seen from Fig. 3 to fail in reproducing the experimental trend, since the so-obtained T_C barely changes with the pressure (blue circles).

In the region between 0–2 GPa, our model has a less accurate agreement with the experimental data, since it predicts a sharper decrease of T_{critical} compared to the observed value. While the estimated trend aligns with the two experimental data points closest to $P = 2$ GPa, the remaining data appear to be in better agreement with the results based solely on volumetric effects (depicted as blue circles in Fig. 4). Intuitively, it sounds reasonable that the hcp structure would withstand some volume contraction before entering the regime of formation of fcc environments, which would imply a slower variation of T_{critical} when $P \to 0$ in comparison to the linear approach employed in our model. We also attribute the fast T_{critical} decline predicted at low pressures to the simplification made of not including pressure effects on the exchange parameters. In an ideal case, we expect that J_0^{hcp} and J_0^{fcc} vary in the intermediate structures. This effect has been neglected since we considered the values from the Sm-type structure which explains the difference between T_{critical} from the model and the hcp phase at zero pressure. This difference makes it also evident how J_0^{hcp} is more susceptible to the formation of stacking faults than to volume effects (by comparison with hcp in different volumes).

Another consequence of taking fixed J_0^{hcp} and J_0^{fcc} values is the inability to predict the collapse of magnetic ordering near the transition to the dhcp phase. Theoretically, one could improve the model by calculating the J_{ij} parameters of intermediate structures between the hcp, the Sm-type, and the dhcp phases. However, the unit cell needed would increase significantly in the number of atoms, rapidly raising the computational effort for the calculation of the exchange parameters.

In experimental reports, dT_C/dP was determined by linear regression of data points in the whole 0–6 GPa interval, obtaining a range 10.6–17.2 K/GPa of values for dT_C/dP [10,11,14–16]; i.e., the change in slope beyond 2 GPa was ignored. If the regression is done separately for the 0–2 GPa and 2–6 GPa regions, we obtain distinct slopes for the respective regions (see Appendix F). This behavior is in line with our hypothesis of the magnetism being critically coupled to the number of stacking faults, which should have different formation rates in these intervals.

Regardless of the mechanism of hcp → Sm-type → dhcp transition description, it implies the presence of at least two phases, either due to spontaneous formation under pressure, growth, or stacking fault accumulation. Since the hcp and the Sm-type phase have very distinct magnetization, we tried to find the fraction (ρ) of hcp phase at each pressure by fitting

$$M_{expt}(P) = \rho M_{hcp}(T) + (1 - \rho) M_{Sm}(T) \tag{5}$$

to the magnetization-pressure data from Ref. [15]. As the temperature associated with the experimental data is unclear, we tried different temperatures in the range between 1–300 K using the magnetization from our Monte Carlo results. However, the results obtained are not comparable with the estimation from volumetric analysis in Ref. [10], which predicts a fraction of Sm-type of about 65% at 2 GPa. In comparison, our closest value was 23%. Notably, the coexistence of distinct magnetic configurations in the phases (hcp, Sm-type, and dhcp) suggests that their interaction gives rise to an intricate magnetic arrangement. It becomes apparent that the experimental drop in magnetization cannot simply be explained by changes in local moments in the individual phases or simple changes in magnetic ordering. A more sophisticated approach which describes the interaction between the magnetic phases is necessary to accurately describe this phenomenon. In order to do so, measurements of the magnetic order of bulk Gd at different pressures would offer important clues for the theoretical modeling. Additionally, due to the strong competition between FM and AFM couplings, it might be beneficial in future studies to include correlation effects modified by pressure on the $4f$ states, to improve the accuracy of the J_{ij} and analyze eventual effects on the magnetic ordering.

IV. CONCLUSIONS

In this work, we investigate the causes for the observed pressure dependence of the magnetic properties of bulk Gd from first-principles calculations. As reported for Nd, another rare-earth element, we observe that the exchange parameters depend on the stacking structure, with the appearance of additional AFM couplings for the Sm-type structure ($9R$) and dhcp. With this in mind, we describe with success the variation of the magnetic order-disorder temperature along the 0–6 GPa pressure range as linearly dependent on the formation of fcc stackings. By doing so, we identify two different T_{critical}/P rates, as a consequence of the different stacking fault formation rates with the pressure associated with the hcp → Sm-type transition and Sm-type → dhcp transitions. Although this behavior change is not considered in previous reports, the experimental data show a similar shift in pressure dependence. We conclude, based on these results, that the structural changes occurring prior to and during the phase transitions of Gd play a major role in the description of the pressure-dependent magnetic properties.

Despite the strong coupling between structure and magnetic properties observed, it was possible to describe the pressure dependence of the Curie temperature reasonably well, considering only the difference of fcc and hcp environments, without including explicitly changes of the J_{ij} parameters induced by variations in the volume.

Moreover, we explored the case of phase coexistence, in which the interaction between phases is simply viewed as an external magnetic field created by the respective magnetization. However, this approximation fails to explain the magnetization dependence on pressure and its collapse close to the transition to the dhcp structure. We link this failure to a more complex magnetic configuration resulting from the coexistence of phases with different magnetic ordering which leads to a competition between AFM and FM alignment of the spins. Our calculations indicate that the dhcp structure may exhibit a complex and frustrated magnetic configuration, requiring further studies. In particular, it might be interesting to search for the magnetic ground state in noncollinear electronic structure calculations. Future research, combining theoretical and experimental approaches, could yield valuable insights into the magnetic behavior of the dhcp phase, potentially uncovering a spin-glass-like state as found in elemental Nd.

ACKNOWLEDGMENTS

R.M.V. would like to thank Anders Bergman for the discussion on magnetically frustrated configurations and Erna K. Delczeg-Czirjak for the support in validation calculations. This work was supported by the Swedish Foundation for Strategic Research, within the project Magnetic Materials for Green Energy Technology (Ref. No. EM16-0039), StandUp, eSSENCE, the Swedish Energy Agency (Energimyndigheten), the Knut and Alice Wallenberg Foundation, the Magnus Ehrnrooth Foundation, the ERC (FASTCORR project), and the Swedish Research Council (VR). The computations performed in this work were enabled by resources provided by the CSC–IT Center for Science, Finland, and by the Swedish National Infrastructure for Computing Centre (SNIC) at the NSC and PDC centers, partially funded by the Swedish Research Council through Grant Agreement No. 2018-05973.

APPENDIX A: THEORETICAL XRPD PATTERNS

To investigate the effect of the accumulation of fcc stacking faults in x-ray powder diffraction (XRPD) patterns, we formulated three theoretical structures with varying ratios of fcc layers between the hcp (0) and Sm-type (1/3) structures. The structures we considered are as in the following patterns (fcc layers in bold): ABA**B**CBC**B** (1/4 fcc and 3/4 hcp), ABA**B**CBCBC**B** (1/5 fcc and 4/5 hcp), and ABA**B**CBCBCBC**B** (1/6 fcc and 5/6 hcp).

We maintained the lattice parameter *a* for the hcp phase and adjusted *c* to match the layer spacing of the hcp structure. Note that the stacking faults are deliberately organized in a periodic manner, making them more detectable in an XRPD pattern. The XRPD pattern of the structures was calculated on VESTA [36] with incident x rays having a wavelength of 0.68825 Å, as in Ref. [11], to ease comparison with experimental data.

The patterns from the different structures can be compared in Fig. 6, and in Fig. 7 we compare the intermediate structure

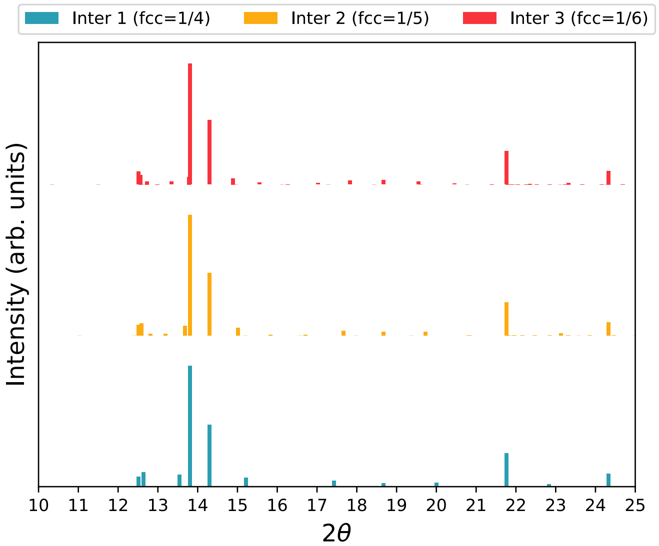

FIG. 6. Predicted x-ray powder diffraction pattern for theoretical structures with ratios of fcc layers between hcp and Sm-type.

with a fcc ratio of 1/6 with the patterns from the hcp and Sm-type structures.

Comparing the patterns of the three intermediate phases in Fig. 6, we observe only slight differences in the major peaks. Mostly, we observe the appearance and splitting of small peaks from the major peaks at 2θ around 12.6 and 13.8. The extent of these splittings increases with the ratio of fcc layers, and is consistent with the splitting of the (100) and (002) reflections of the hcp structure in the XRPD pattern of the Sm-type structure. However, these differences should be too subtle to be observed experimentally since the peak

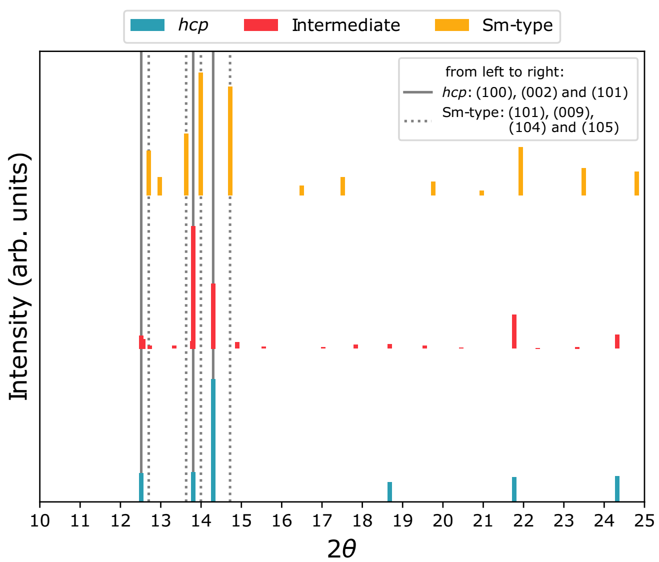

FIG. 7. Comparison between predicted x-ray powder diffraction patterns for hcp, Sm-type, and a theoretical intermediate structure of gadolinium. The intermediate structure is designed to have a ratio of hcp (5/6) and fcc (1/6) layers in the middle of hcp and Sm-type (2/3 fcc) structures. Main low-angle reflections of the hcp (Sm-type) structure are represented by vertical solid (dotted) planes.

broadening would conceal the differences. As a result, we only need to compare one of the proposed structures with the hcp and Sm-type structures without loss of generality.

In Fig. 7 it becomes evident that the major peaks of the intermediate phase share features to the patterns of both hcp and Sm-type, with no major peak that could exclusively be attributed to the intermediate phase. The broadening of the peaks measured in experiments would make the task even more difficult, since the relative intensities become less clear, as is evidenced in the patterns obtained in Ref. [11]. Moreover, peak width increases in experiments when more than two phases are present. Therefore, distinguishing any combination of hcp and Sm-type phases with the intermediate phase becomes virtually impossible.

In light of these observations, we conclude that previously reported XRPD patterns are not conclusive on the formation and accumulation of fcc stacking faults in structural transformations under pressure.

APPENDIX B: HUBBARD-I APPROXIMATION

The treatment of correlation effects on f states is a persistent topic in the literature concerning rare-earth-based compounds, owing to their significance in structural, electronic, and magnetic properties. One of the central challenges in DFT calculations of these compounds lies in accurately capturing the (de)localization of f states, a task that standard DFT often struggles with. For instance, in metallic Gd, this deficiency manifests as a small occupation of $4f$ states at the Fermi energy, favoring an AFM phase over a FM phase [4] as the ground state.

Various strategies have been devised to address this issue, ranging from treating f as core states to employing methods like DFT+U and DMFT, each increasing in complexity [3,4]. While the former approaches excel in predicting the system's properties under no applied pressure, they fall short in capturing strong correlation effects enhanced by pressure. The literature suggests that pressure promotes the delocalization of f states, enhancing correlation effects and leading to the observed volume collapse in rare-earth metals under high pressures [17,42]. In such scenarios, combining DMFT with more conventional DFT methods such as L(S)DA emerges as a more robust choice for an accurate electronic structure description [43].

The Hubbard-I approximation (HIA) [44] is a variant of DFT+DMFT tailored to describe correlated d and f states, proving particularly effective in modeling rare-earth elemental systems, where $4f$ states exhibit localized behavior [3,43,45]. In this approach, an explicit Coulomb interaction interaction term U is introduced, augmenting the Coulomb repulsion between orbitals. This interaction is tackled within DMFT as an Anderson impurity problem [3].

To explore the potential delocalization of $4f$ states within the pressure range of 0–6 GPa, we computed the hybridization function $\Delta(E)$ for these states using the HIA method as implemented in RSPt [3,46]. The interorbital (spd) contribution to the exchange energy of the $4f$ states was approximated with a Stoner-like model (more details in Ref. [46]). We took the exchange splitting calculated within the open-core approximation (for the $P = 0$ GPa case) as a reference for the

TABLE III. Projected spin magnetic moments for $4f$ and $3d$ calculated with Hubbard I approximation.

$S\ (\mu_B)$	$P = 0$ GPa	$P = 2$ GPa	$P = 6$ GPa
$4f$	6.85	6.84	6.84
$3d$	0.49	0.47	0.41

parametrization of this model. In the HIA method, $\Delta(E)$ characterizes the perturbation caused in the system by introducing an impurity (in this case, the $4f$ electrons) within a medium comprising the remaining electrons, serving as a proxy measure of the impurity localization, as detailed in Ref. [45]. The calculations were conducted for the hexagonal-close-packed (hcp) structure of Gd under three different pressures (0, 3, and 6 GPa), assuming exclusively volumetric effects on the structure. Hubbard parameters $U = 6.7$ eV and $J = 0.7$ eV [4] were chosen for consistency with the performed L(S)DA+U calculations.

Within the considered pressure range, our calculations reveal a negligible impact of pressure on the f-projected spin magnetic moment, as demonstrated in Table III. While not definitive, these findings suggest that the $4f$ states remain localized, as one would anticipate a transfer of spin moment from the $4f$ orbitals to the remaining orbitals (s, p, and d) if delocalization were occurring.

Examining the hybridization functions in Fig. 8, we note a modest increase in the hybridization of the f states with the surrounding medium, indicating a slight tendency toward delocalization [45]. However, despite this observed increase, the maximum value of the hybridization function below the Fermi energy (Δ_{max}) remains small compared to Ce-based reference systems exhibiting either weak (α-Ce) or stronger itinerant behavior ($CePt_3$). When compared with Gd-based monopnictides, we find that Δ_{max} falls within the same order of magnitude as that of GdBi and GdSb, which show

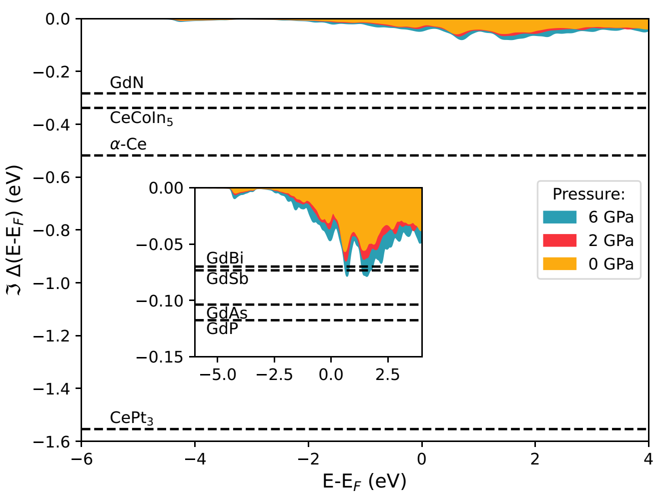

FIG. 8. Imaginary component of the hybridization function, calculated for the $4f$ orbitals of hcp Gd under different pressures. Reference values from Ref. [45] for the maximum of Δ below the Fermi energy for other rare-earth-based compounds are represented in horizontal lines.

TABLE IV. Pressure-dependent mean-field T_C calculated using the HIA and open-core approximation to describe the $4f$ states of hcp Gd. The HIA+CPA refers to an $f^6_{x/2}f^7_{1-x}f^8_{x/2}$ mixture in the occupation of the $4f$ states (more details in the text).

Mean-field T_C (K)	$P = 0$ GPa	$P = 2$ GPa	$P = 6$ GPa
Open-core approximation	350	336	321
HIA	343	336	294
HIA+CPA ($x = 0.01$)		335	299
HIA+CPA ($x = 0.04$)		327	287
HIA+CPA ($x = 0.10$)		311	260

hints of being localized states [45]. In Ref. [45] a consistent $\Delta_{\max}$ across the monopnictides series was reported, despite variations in the unit cell volume, a behavior attributed to state localization. Moreover, we highlight that Δ calculated under pressure remains in the same order of magnitude for the pressure-free system, which is well established in the literature to have very localized f states [3,47].

Due to their small order of magnitude, J_{ij} parameters can be sensible to minor variations in the localization of f states. Thus we proceeded with the calculation of the J_{ij} within the HIA and open-core approximation (here in the fully relativistic description and using the muffin-tin heads projection [29] to assure equal footing with HIA, in contrast with the calculation in the main text) and to compute the respective mean-field T_C. Comparing these results, in Table IV, we observe that the introduction of correlation by HIA has a small effect in the pressure dependence of T_C inducing a slightly faster drop of the critical temperature. However, such effect is not comparable with the variation induced by the structural transformation (see Fig. 3).

By construction, the HIA does not include hybridization effects between the impurity (in this case, the $4f$ states) and the rest of the system [43,44]. In particular, HIA results neglect the increase in the hopping of electrons in/out of f states, a phenomenon associated with delocalization. The hopping of electrons from and to the bath, mostly formed by the *spd* states, changes the occupancy of f states from $4f^7$ to $4f^8$ (one electron hops in) and $4f^6$ (one electron hops out), respectively. According to Hund's rule, the spin moment arising from the $4f$ states is maximum for f^7, implying that changes in the f occupancy via hopping can screen the spin moment of these orbitals. Since the intra-atomic exchange between $4f$ and *spd* states is considered on the mean-field level, the main effects on the J_{ij} parameters are due to the alterations on the local $4f$ moment. Thus, a potential screening of the $4f$ moment can induce a weakening of the exchange parameters and, therefore, lower the order-disorder temperature.

To estimate the impact of such effects in the J_{ij} parameters, we performed additional HIA calculations with f states described within the coherent potential approximation (CPA) as a mixture of f states with different occupations: f^6, f^7, and f^8. These calculations were carried out by taking advantage of the Green's function machinery implemented in RSPt [43,46], which is also used to map the effective impurity model in HIA. Analogously to CPA, the local Green's function for the $4f$ states is set to a weighted average (by the respective concentrations) of the virtual Green's functions for each f occupation considered. For simplification, we considered only the case where these excited configurations are equiprobable, with the $4f$ states being then given by the mixture $f^6_{x/2}f^7_{1-x}f^8_{x/2}$.

Note that in this description, we do not treat the hopping electrons between states as a dynamical effect since concentrations of $4f^6$ and $4f^8$ are kept fixed. Instead, we focus on the change in the f states' occupancy as a static phenomenon, thus likely overestimating the screening of the magnetic moment induced by hybridization of the f orbitals with the *spd* bath.

To get close to a realistic physical picture, the x value (concentration of f^6 plus f^8 states) was chosen to be small, to which we consider initially $x = 0.01$ and $x = 0.04$. As shown in Table IV, this treatment has a small impact on the mean-field Curie temperature computed from the respective J_{ij} calculations. The increase of $4f^6$ and $4f^8$ concentrations leads, as expected, to a slight decrease of the spin moment and overall, the same trend is observed for the Curie temperature but is not comparable to the experimental observations (see Fig. 3) [15]. An unrealistic high concentration of these configurations ($x = 0.1$) is necessary to approach the T_C variation measured, taking as reference earlier theoretical studies and experimental observations for lighter rare-earth metals [42,48].

Our HIA calculations support the notion that within the pressure range of 0–6 GPa, there are no significant alterations in the localization of the f states in the hcp structure. These conclusions align with prior DMFT calculations conducted for lighter rare-earth metals [42,48]. While previous works [42,48] have highlighted pressure-induced delocalization of f states for high pressures, at lower pressures (<10 GPa) as in our findings, it was found that f states remain largely unaffected. Hence, in line with other studies [9,13], we conclude that for the pressure range of 0–6 GPa, adopting a corelike treatment of f states in the electronic structure calculations conducted in this study does not compromise accuracy.

APPENDIX C: ENTHALPY

The assumption of a linear formation of stacking faults along pressure was tested with the enthalpy curves calculated for the hcp and Sm-type structures. To accomplish this, we computed energy-volume curves for both structures using the PBE [49] exchange-correlation potential (motivated by a better performance in describing the structural properties [3]). Afterward, we fitted the Murnaghan equation of state [50] to obtain the enthalpy values. Analyzing the calculated enthalpy, we identified the pressure at which the Sm-type structure becomes stable to be approximately 3.34 GPa, close to the experimental values.

Under the hypothesis that the structural transition is driven by the accumulation of fcc stacking faults, we associated the enthalpy at this pressure point with the energy required to form three stacking faults. Assuming a constant energy cost for creating a single stacking fault (leading to the linear relation), we pinpointed the enthalpy values on the hcp curve, which correspond to the formation of the first and second fcc layers. We then performed a linear regression on the identified points, as depicted in Fig. 9. Based on the results of this

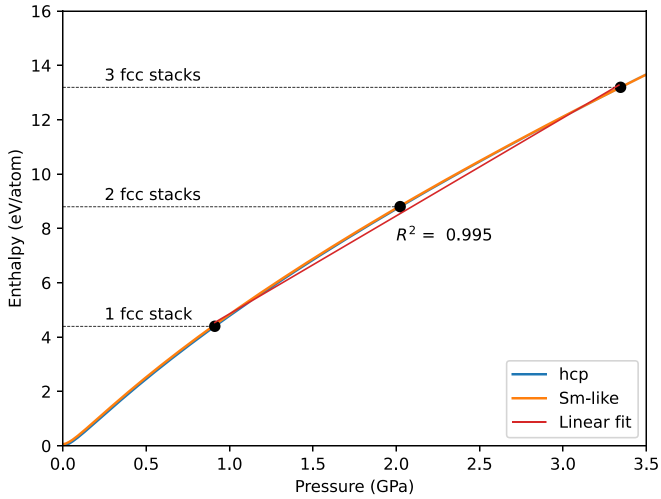

FIG. 9. Verification of linear assumption on the formation of stacking faults between hcp → Sm-like phases from respective enthalpy curves.

regression and the corresponding coefficient of determination, we can reasonably conclude that the assumption of a linear progression of stacking faults with increasing pressure is a reasonable approximation.

APPENDIX D: MAGNETIC CONFIGURATION OF THE DHCP STRUCTURE

The exchange parameters for the dhcp calculated for a sample of magnetic configurations are presented in Fig. 10. The different sets present a similar behavior with slight variations in the magnitude of the couplings, with AFM (1-layer, ↑↓↑↓) configurations deviating more from the remaining. Due to the strong competition between AFM and FM couplings, the small deviations result in very different magnetic configurations in the Monte Carlo simulations as seen in Fig. 11.

APPENDIX E: HEAT CAPACITY

Figure 12 shows the temperature-dependent magnetic heat capacity (C) calculated in Monte Carlo simulations with

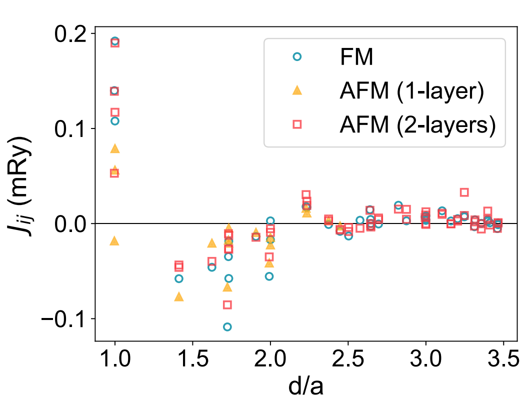

FIG. 10. Exchange parameters for Gd in the dhcp structure obtained under different magnetic configurations.

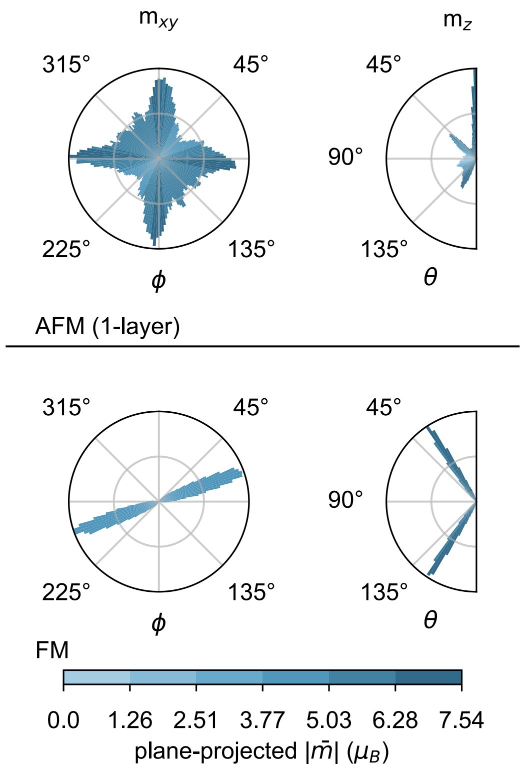

FIG. 11. Statistical distribution of spin directions (spherical coordinates with azimuthal angle ϕ in the x-y plane and polar angle θ) for different Gd systems simulated $T = 1$ K with UppASD. The bars are colored according to the average magnetic moment (projected in the respective x-y or z plane) of the spins aligned in the respective direction.

UppASD. To calculate the heat capacity, we used the thermodynamic relation

$$C = \frac{\partial \langle E \rangle}{\partial T}, \tag{E1}$$

where E is the energy evaluated from the Heisenberg Hamiltonian [see Eq. (1)]. The peaks in the calculated heat

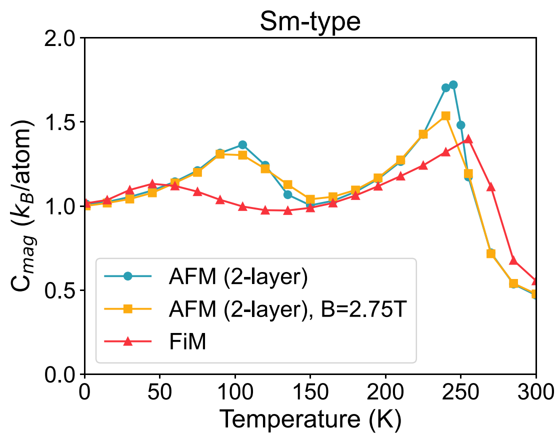

FIG. 12. Magnetic heat capacity and computed from Monte Carlo simulations for Gd in the Sm-type structure.

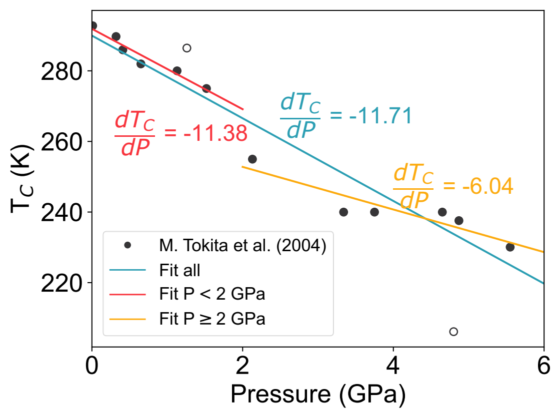

FIG. 13. Comparison of linear fits for different pressure intervals. The resultant dT_C/dP varies significantly if a different fit is made for the hcp and Sm-type phases. Experimental data from [15].

capacity are used as a reference for the magnetic ordering temperature.

APPENDIX F: LINEAR FIT

In Fig. 13, we compare the dT_C/dP ratio obtained for different linear fits of recent experimental data [15]. Two cases are considered: when all data points in the 0–6 GPa data range are included, and the separate fits for the 0–2 GPa and 2–6 GPa ranges. We observe that the dT_C/dP obtained by fitting solely to the 2–6 GPa is considerably smaller (in magnitude) than the analogous calculations in the 0–2 GPa. Consequently, by fitting all the data points simultaneously, the change in the trend is missed, and the resulting dT_C/dP follows the trend of the 0–2GPa, where this ratio is sharper.

The different dT_C/dP imply that the magnetic properties vary differently according to the implied structures, highlighting that the magnetism of Gd has structure-intrinsic properties.

[1] K. A. Gschneidner and L. Eyring, *Handbook on the Physics and Chemistry of Rare Earths* (Elsevier, Amsterdam, 1978), Vol. 1.

[2] J. Jensen and A. R. Mackintosh, *Rare Earth Magnetism* (Clarendon Press, Oxford, 1991).

[3] I. L. Locht, Y. O. Kvashnin, D. C. Rodrigues, M. Pereiro, A. Bergman, L. Bergqvist, A. I. Lichtenstein, M. I. Katsnelson, A. Delin, A. B. Klautau, B. Johansson, I. Di Marco, and O. Eriksson, Standard model of the rare earths analyzed from the Hubbard I approximation, Phys. Rev. B **94**, 085137 (2016).

[4] I. Turek, J. Kudrnovský, G. Bihlmayer, and S. Blügel, Ab initio theory of exchange interactions and the Curie temperature of bulk Gd, J. Phys.: Condens. Matter **15**, 2771 (2003).

[5] L. M. Sandratskii and J. Kübler, Local magnetic moments of conduction electrons in gadolinium, Europhys. Lett. **23**, 661 (1993).

[6] L. M. Sandratskii, Exchange splitting of surface and bulk electronic states in excited magnetic states of Gd: First-principles study, Phys. Rev. B **90**, 184406 (2014).

[7] M. Colarieti-Tosti, S. I. Simak, R. Ahuja, L. Nordström, O. Eriksson, D. Åberg, S. Edvardsson, and M. S. S. Brooks, Origin of magnetic anisotropy of Gd metal, Phys. Rev. Lett. **91**, 157201 (2003).

[8] R. M. Vieira, O. Eriksson, T. Björkman, A. Bergman, and H. C. Herper, Realistic first-principles calculations of the magnetocaloric effect: Applications to hcp Gd, Mater. Res. Lett. **10**, 156 (2022).

[9] Q. Li, H. Ehteshami, K. Munro, M. Marqués, M. I. McMahon, S. G. MacLeod, and G. J. Ackland, Nonexistence of the *s*-*f* volume-collapse transition in solid gadolinium at pressure, Phys. Rev. B **104**, 144108 (2021).

[10] N. Golosova, D. Kozlenko, E. Lukin, S. Kichanov, and B. Savenko, High pressure effects on the crystal and magnetic structure of ^{160}Gd metal, J. Magn. Magn. Mater. **540**, 168485 (2021).

[11] M. Mito, Y. Kimura, K. Yamakata, M. Ohkuma, H. Chayamichi, T. Tajiri, H. Deguchi, and M. Ishizuka, Relationship of magnetic ordering and crystal structure in the lanthanide ferromagnets Gd, Tb, Dy, and Ho at high pressures, Phys. Rev. B **103**, 024444 (2021).

[12] E. Mendive-Tapia and J. B. Staunton, Theory of magnetic ordering in the heavy rare earths: *Ab initio* electronic origin of pair- and four-spin interactions, Phys. Rev. Lett. **118**, 197202 (2017).

[13] G. K. Samudrala, G. M. Tsoi, S. T. Weir, and Y. K. Vohra, Structural and magnetic phase transitions in gadolinium under high pressures and low temperatures, High Press. Res. **34**, 385 (2014).

[14] D. D. Jackson, V. Malba, S. T. Weir, P. A. Baker, and Y. K. Vohra, High-pressure magnetic susceptibility experiments on the heavy lanthanides Gd, Tb, Dy, Ho, Er, and Tm, Phys. Rev. B **71**, 184416 (2005).

[15] M. Tokita, K. Zenmyo, H. Kubo, K. Takeda, M. Mito, and T. Iwamoto, RKKY interaction in metallic Gd in GPa pressure regions, J. Magn. Magn. Mater. **272-276**, 593 (2004).

[16] T. Iwamoto, M. Mito, M. Hidaka, T. Kawae, and K. Takeda, Magnetic measurement of rare earth ferromagnet gadolinium under high pressure, Phys. B: Condens. Matter **329-333**, 667 (2003).

[17] D. B. McWhan and A. L. Stevens, Effect of pressure on the magnetic properties and crystal structure of Gd, Tb, Dy, and Ho, Phys. Rev. **139**, A682 (1965).

[18] B. Coles, Transformation effects, stacking faults and magnetism in the light rare earths, J. Magn. Magn. Mater. **15-18**, 1225 (1980).

[19] W. A. Grosshans and W. B. Holzapfel, Atomic volumes of rare-earth metals under pressures to 40 GPa and above, Phys. Rev. B **45**, 5171 (1992).

[20] J. M. Wills, O. Eriksson, P. Andersson, A. Delin, O. Grechnyev, and M. Alouani, *Full-Potential Electronic Structure Method*, Springer Series in Solid-State Sciences (Springer, Berlin, 2010), Vol. 167.

[21] J. P. Perdew and Y. Wang, Accurate and simple analytic representation of the electron-gas correlation energy, Phys. Rev. B **45**, 13244 (1992).

[22] T. Björkman, CIF2Cell: Generating geometries for electronic structure programs, Comput. Phys. Commun. **182**, 1183 (2011).

[23] J. Korringa, On the calculation of the energy of a Bloch wave in a metal, Physica **13**, 392 (1947).

[24] W. Kohn and N. Rostoker, Solution of the Schrödinger equation in periodic lattices with an application to metallic lithium, Phys. Rev. **94**, 1111 (1954).

[25] H. Ebert, D. Ködderitzsch, and J. Minár, Calculating condensed matter properties using the KKR–Green's function method: Recent developments and applications, Rep. Prog. Phys. **74**, 096501 (2011).

[26] P. Soven, Coherent-potential model of substitutional disordered alloys, Phys. Rev. **156**, 809 (1967).

[27] G. M. Stocks, W. M. Temmerman, and B. L. Gyorffy, Complete solution of the Korringa-Kohn-Rostoker coherent-potential-approximation equations: Cu-Ni alloys, Phys. Rev. Lett. **41**, 339 (1978).

[28] A. I. Liechtenstein, V. I. Anisimov, and J. Zaanen, Density-functional theory and strong interactions: Orbital ordering in Mott-Hubbard insulators, Phys. Rev. B **52**, R5467 (1995).

[29] Y. O. Kvashnin, R. Cardias, A. Szilva, I. Di Marco, M. I. Katsnelson, A. I. Lichtenstein, L. Nordström, A. B. Klautau, and O. Eriksson, Microscopic origin of Heisenberg and non-Heisenberg exchange interactions in ferromagnetic bcc Fe, Phys. Rev. Lett. **116**, 217202 (2016).

[30] A. Liechtenstein, M. Katsnelson, V. Antropov, and V. Gubanov, Local spin density functional approach to the theory of exchange interactions in ferromagnetic metals and alloys, J. Magn. Magn. Mater. **67**, 65 (1987).

[31] B. Skubic, J. Hellsvik, L. Nordström, and O. Eriksson, A method for atomistic spin dynamics simulations: Implementation and examples, J. Phys.: Condens. Matter **20**, 315203 (2008).

[32] O. Eriksson, A. Bergman, L. Bergqvist, and J. Hellsvik, *Atomistic Spin Dynamics* (Oxford University Press, Oxford, 2017), Vol. 1.

[33] J. Perez-Mato, S. Gallego, E. Tasci, L. Elcoro, G. de la Flor, and M. Aroyo, Symmetry-based computational tools for magnetic crystallography, Annu. Rev. Mater. Res. **45**, 217 (2015).

[34] E. Y. Tonkov, I. L. Aptekar, V. F. Degtareva, and Y. I. Krasavin, Conversion of the metastable high-pressure phase of Gd, Tb, Dy, and Ho into the stable phase, Sov. Phys. Dokl. **21**, 9 (1976).

[35] A. Nakaue, Studies on the pressure-temperature phase diagram of Nd, Sm, Gd and Dy, J. Less-Common Met. **60**, 47 (1978).

[36] K. Momma and F. Izumi, VESTA3 for three-dimensional visualization of crystal, volumetric and morphology data, J. Appl. Crystallogr. **44**, 1272 (2011).

[37] U. Kamber, A. Bergman, A. Eich, D. Iuşan, M. Steinbrecher, N. Hauptmann, L. Nordström, M. I. Katsnelson, D. Wegner, O. Eriksson, and A. A. Khajetoorians, Self-induced spin glass state in elemental and crystalline neodymium, Science **368**, eaay6757 (2020).

[38] M. Mito, K. Matsumoto, Y. Komorida, H. Deguchi, S. Takagi, T. Tajiri, T. Iwamoto, T. Kawae, M. Tokita, and K. Takeda, Volume shrinkage dependence of ferromagnetic moment in lanthanide ferromagnets gadolinium, terbium, dysprosium, and holmium, J. Phys. Chem. Solids **70**, 1290 (2009).

[39] Y. O. Kvashnin, O. Grånäs, I. Di Marco, M. I. Katsnelson, A. I. Lichtenstein, and O. Eriksson, Exchange parameters of strongly correlated materials: Extraction from spin-polarized density functional theory plus dynamical mean-field theory, Phys. Rev. B **91**, 125133 (2015).

[40] UppASD, Department of Physics and Astronomy, Uppsala University, Sweden, https://www.physics.uu.se/research/materials-theory/ongoing-research/uppasd/.

[41] L. Bellaiche and D. Vanderbilt, Virtual crystal approximation revisited: Application to dielectric and piezoelectric properties of perovskites, Phys. Rev. B **61**, 7877 (2000).

[42] A. K. McMahan, Combined local-density and dynamical mean field theory calculations for the compressed lanthanides Ce, Pr, and Nd, Phys. Rev. B **72**, 115125 (2005).

[43] O. Grånäs, I. Di Marco, P. Thunström, L. Nordström, O. Eriksson, T. Björkman, and J. M. Wills, Charge self-consistent dynamical mean-field theory based on the full-potential linear muffin-tin orbital method: Methodology and applications, Comput. Mater. Sci. **55**, 295 (2012).

[44] A. I. Lichtenstein and M. I. Katsnelson, *Ab initio* calculations of quasiparticle band structure in correlated systems: LDA++ approach, Phys. Rev. B **57**, 6884 (1998).

[45] H. C. Herper, T. Ahmed, J. M. Wills, I. Di Marco, T. Björkman, D. Iuşan, A. V. Balatsky, and O. Eriksson, Combining electronic structure and many-body theory with large databases: A method for predicting the nature of 4*f* states in Ce compounds, Phys. Rev. Mater. **1**, 033802 (2017).

[46] L. Peters, I. Di Marco, P. Thunström, M. I. Katsnelson, A. Kirilyuk, and O. Eriksson, Treatment of $4f$ states of the rare earths: The case study of TbN, Phys. Rev. B **89**, 205109 (2014).

[47] P. Kurz, G. Bihlmayer, and S. Blügel, Magnetism and electronic structure of hcp Gd and the Gd(0001) surface, J. Phys.: Condens. Matter **14**, 6353 (2002).

[48] A. K. McMahan, R. T. Scalettar, and M. Jarrell, Screening of $4f$ moments and delocalization in the compressed light rare earths, Phys. Rev. B **80**, 235105 (2009).

[49] J. P. Perdew, K. Burke, and M. Ernzerhof, Generalized gradient approximation made simple, Phys. Rev. Lett. **77**, 3865 (1996).

[50] F. D. Murnaghan, The compressibility of media under extreme pressures, Proc. Natl. Acad. Sci. USA **30**, 244 (1944).